Microsystem Technologies 9 (2002) 87–91 © Springer-Verlag 2002
DOI 10.1007/s00542-002-0199-1

Characterization of electroplated nickel

T. Fritz, H. S. Cho, K. J. Hemker, W. Mokwa, U. Schnakenberg

Abstract Properties of electroplated nickel such as crystallographic texture, Young's modulus, strength and microstructure strongly depend on the parameter mean current density used for electrodeposition. By means of micro tensile testing mechanical material parameters were determined. At low mean current density (2 mA/cm^2) brittle layers with high Young's modulus and high strength were obtained, whereas at high current density (15 mA/cm^2) ductile layers with low Young's modulus and low strength were deposited.

1 Introduction

Electroplated nickel is a promising material to realize movable structures for micro-electro-mechanical-systems (MEMS) applications [1]. Movable structures in nickel can simply be made using a sacrificial layer etching technique [2, 3].

Materials for movable micro structures have to be well characterized with respect to mechanical parameters. A high modulus of elasticity and elastic behavior over a wide mechanical strain range is required [4]. Nickel-based structures fulfill the requirements [1]. Electroplated nickel structures show a dependency of plating parameters on texture and mechanical properties [5, 6].

Received: 10 August 2001/Accepted: 24 September 2001

T. Fritz (✉), W. Mokwa, U. Schnakenberg
Institute of Materials in Electrical Engineering I Aachen
University of Technology (RWTH Aachen),
Sommerfeldstrasse 24,
D-52074 Aachen, Germany

H. S. Cho, K. J. Hemker
Departments of Mechanical Engineering and Materials Science,
The John Hopkins University, Baltimore MD, USA

Parts of the work were carried out within the project ELMINOS, which is supported by the state of North Rhine-Westphalia, Germany. The equipment used for the experiments was funded by the state of North Rhine-Westphalia. We would like to express our sincere gratitude to Mirko Hofmann for his assistance in performing the measurements of indentation hardness. The participation of Cho and Hemker was sponsored by the Defense Advanced Research Projects Agency (DARPA) and Air Force Research Laboratory, Air Force Material Command, USAF, under agreement number F30602-99-2-0553.

This paper was presented at the Fourth International Workshop on High Aspect Ratio Microstructure Technology HARMST 2001 in June 2001.

This paper presents a detailed investigation of the influence of the deposition parameters on texture, structure, Young's modulus, strength and indentation hardness of electroplated nickel.

2 Experimental

For the fabrication of the micro structured nickel layers passivated 100 mm silicon wafers were used as substrates. They were evaporated with a 50 nm thick titanium and an 100 nm thick gold layer, respectively serving as a plating base. After a lithography step nickel was electrodeposited in a nickel sulphamate based electrolyte (Nickelsulfamat EL, Polyclad Enthone OMI, Germany) without brightener additives. The pH of the electrolyte was adjusted to 3.2 and the temperature to 40 °C, respectively. The electrolyte contains no chloride but bromide for anode activation. The wetting agent (Netzmittel K) was fixed to 5 ml/l. Pulse-plating (PP) was applied ($T_{on} = 5$ ms; $T_{off} = 5$ ms) using pulse plating equipment (Dynatronix, Type DPR-20-5-10). Depositions with 15 μm layer thickness were carried out with different mean current-densities (2.5; 5.0; 10.0 and 20.0 mA/cm^2 indicated by A to D, see Table 1). In addition depositions with mean current-densities of 2.0 and 15.0 mA/cm^2 (indicated by E and F, see Table 1) were carried out providing dog-bone shaped 140 μm thick micro tensile samples with self-aligning ends and a gage cross-section of 140 × 250 μm.

X-ray diffractometry (XRD) measurements with Bragg-Brentano geometry ($\theta/2\theta$-measurements) (Type Phillps PW 3010) were carried out determine the preference orientation of the substrate layers and of the electroplated nickel layers, respectively. For the discussion of change of peak intensities they were transformed to relative intensities using the values of an isotropic polycrystalline nickel sample (Goodfellow, Type NI1000620, high purity: 99.99+%, measured relative intensities $I_{(111)}/I_{(200)}/I_{(220)} = 100/46/26$) comparable to [7]. In addition, texture analysis of the samples E and F were carried out. The spatial distribution of three characteristic crystal planes ({1 1 1}, {2 0 0} and {2 2 0}) of the face centered cubic nickel (fcc) lattice was investigated with a four-circle texture goniometer (Type Seifert PTS 3000). Measurements of Vickers indentation hardness (HV) were carried out on all discussed nickel layers. Samples A to D were measured using a force equivalent of 100 g, whereas a 500 g force equivalent was used for E and F, respectively.

The structure analysis of the samples E and F was supported by taking SEM-pictures of polished and

electrochemically etched cross sections. The cross sections were etched anodically in diluted sulfuric acid for 10 s at 3 V.

The micro tensile samples from deposition E and F were released from the substrate. Top and bottom faces were mechanically polished to a mirror surface. A 3 μm deep microhardness indents were placed 300 μm apart in the center of the gage, serving as reflective markers for an interferometric strain/displacement gage (ISDG). This non-contact optical technique was used to measure strain in the specimen with an accuracy of a strain resolution of ∼5 microstrain [8, 9]. Loading is accomplished through the use of a piezo-electric actuator that allows for precise displacement controlled experiments, and the tensile tests were conducted at a constant strain rate of 3×10^{-4} s^{-1}. The micro tensile samples were pulled in tension until obvious plastic deformation had occurred. They were unloaded and reloaded several times so that the Young's modulus could be measured and compared with the final unloading that occurs at the end of the test. For each deposition E and F two micro tensile samples were examined.

Table 1. Layer thickness d, mean current densities j, and relative intensities of the measured (1 1 1), (2 0 0), (2 2 0) $\theta/2\theta$-XRD peak intensities of samples A to F

Sample	d [μm]	j [mA/cm^2]	(1 1 1)	(2 0 0)	(2 2 0)
A	15	2.5	0.13	0.14	7.04
B	15	5.0	0.13	1.56	2.90
C	15	10.0	0.12	2.57	0.00
D	15	20.0	0.14	2.54	0.00
E	140	2.0	1.36	0.48	1.08
F	140	15.0	0.13	2.44	0.32

3 Results

The gold layers served as plating base in all depositions show a (1 1 1) crystalline preference orientation [3].

Figure 1 shows $\theta/2\theta$-measurements of the samples A to D and the samples E and D. The reduced peak intensities as well as the applied mean current densities are summarized in Table 1. Regarding to the samples A to D the intensity of the (2 2 0) peak decreases, whereas the (2 0 0) peak intensity increases with increasing mean current density. At low mean current density of 2.5 mA/cm^2 the intensity of the (2 2 0) peak is most enlarged, whereas at the high mean current densities of 10 and 20 mA/cm^2 the (2 0 0) peak intensity show the largest values (see Table 1). In comparison, the (1 1 1) peak intensity does not change significantly with respect to the variation of the mean current density.

The $\theta/2\theta$-XRD plots of the layer F deposited with a mean current density between sample C and D of 15 mA/cm^2 is in good accordance with those of C and D. Sample E deposited with a mean current density of 2 mA/cm^2 shows a dominating (1 1 1)-peak. The reduced peak intensities indicate a rather statistically oriented sample with a weak enlarged (2 2 0)-peak.

The result of texture analysis of samples E and F are depicted in Fig. 2. In both cases pure fiber textures were found. In this case the rotational symmetric pole-figures can be reduced to two dimensional cuts representing ψ-scans of the {1 1 1}-, {2 0 0}- and {2 2 0}-planes. The ψ-scans display the reflex intensity of a particular plane with respect to the samples angle of inclination. The ψ-scans of sample E show half circular pattern for all three measured planes which is caused by a high amount of statistically oriented crystallites. A small amount of

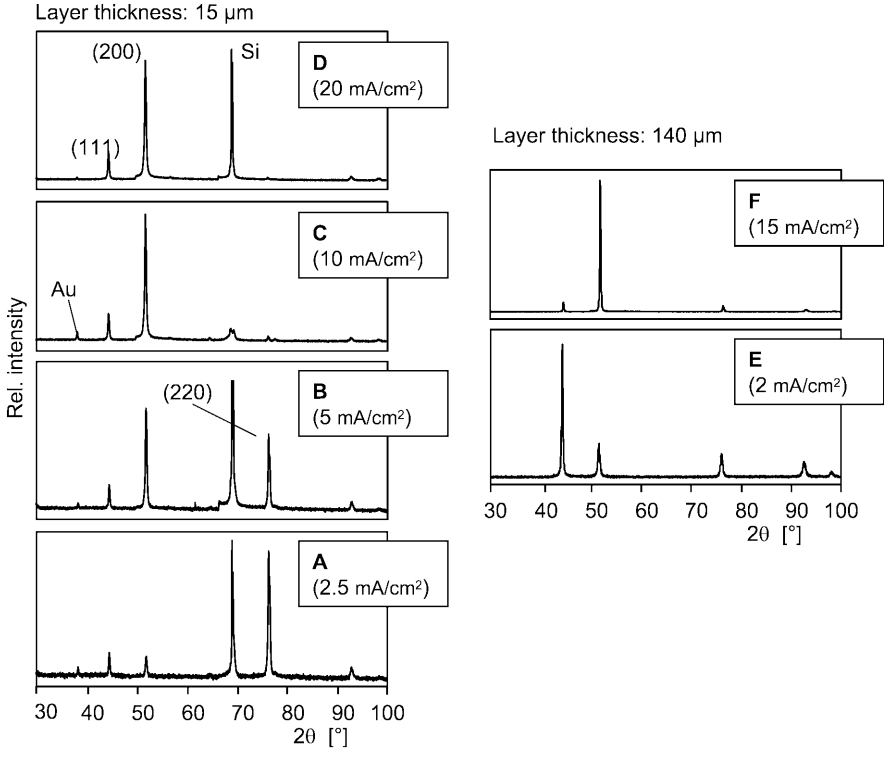

Fig. 1. XRD $\theta/2\theta$-scans of electroplated nickel for different mean current densities. Layer thickness of sample A to D are 15 μm and 140 μm of samples E and F, respectively

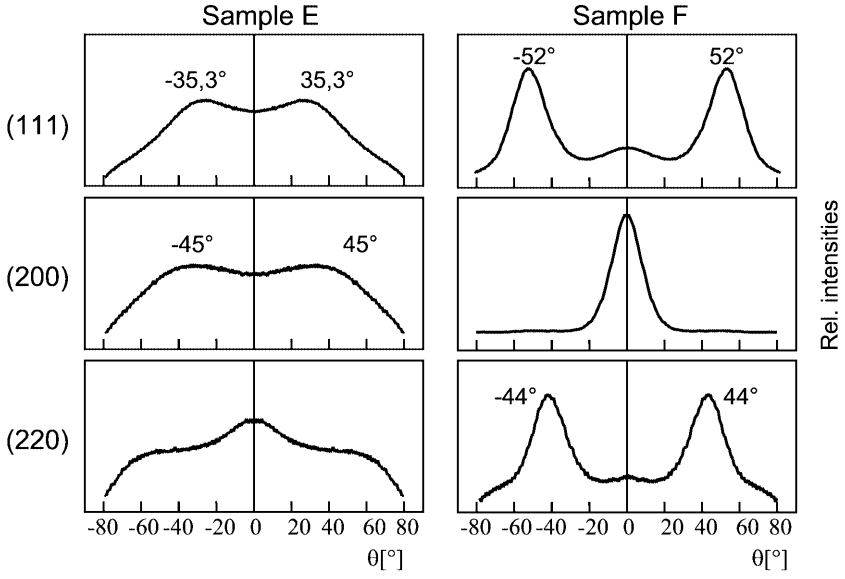

Fig. 2. Ψ-scans from texture analysis of sample E and F. Depicted are reflex intensities of the (1 1 1)-, (2 0 0)-, and (2 2 0)-planes with respect to the tilt angle of the samples

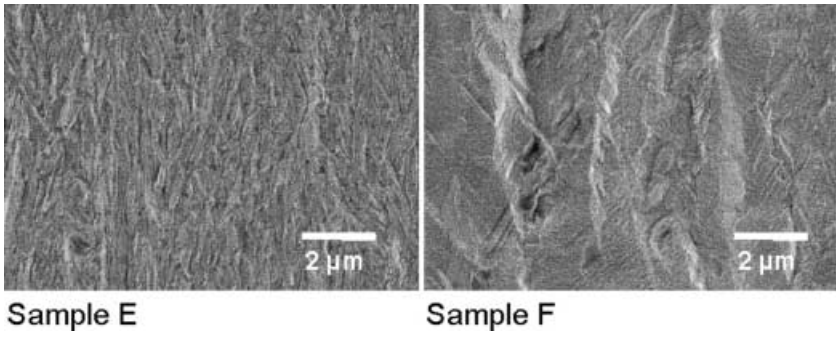

Fig. 3. SEM-photographs of electrochemically etched cross sections of samples E and F

⟨2 2 0⟩-oriented crystallites is indicated by peaks at 0° for {2 2 0}-, ±45.0° for {2 0 0}- and ±35.3° for {1 1 1}-planes. In extension to the $\theta/2\theta$-XRD-diagrams (see Fig. 1) a weak but clearly visible ⟨2 2 0⟩-texture was found in sample E. Sample F shows a sharp peak at 0° in ψ-scan of {2 0 0}-plane whereas ψ-scans of the {1 1 1}- and {2 2 0}-planes show two peaks at ±54.5° and ±45.0°, respectively. These results are in good agreement with the $\theta/2\theta$-measurement of sample F indicating a strong and less dispersed ⟨2 2 0⟩-texture. Both samples show crystallographic anisotropy resulting from fiber-textures.

The electrochemically etched cross sections of sample E and F show different structures (Fig. 3). Sample E shows a fine grained structure with columnar portions in direction of layer growth. The grain size is much smaller than 1 µm. In contrast, large crystallites can be found in the cross section of sample F. The grain size is in the range of some microns. Etch lines diagonal to the direction of growth can be observed.

The values for Vickers hardness (HV) are shown in Fig. 4. Regarding to samples A to D (layer thickness 15 µm units, HV0.1) the highest value corresponds to the layer deposited with the lowest mean current density. The hardness decreases continuously with increasing mean current density. The obtained values of the 140 µm thick samples E and F (units HV0.5) fit well to the general tendency. Sample E has an indentation hardness which is about two times higher compared to sample F.

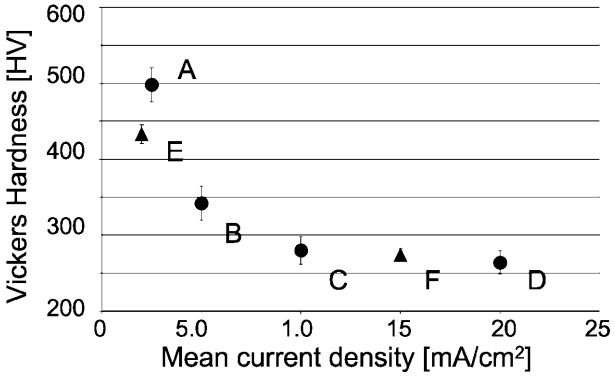

Fig. 4. Vickers indentation hardness of samples A to F. Units of indentation hardness A–D: HV0.1 (circles), E and F: HV0.5 (triangles). Standard deviation of 20 single measurements is indicated

In Fig. 5 typical stress strain diagrams of samples E and F are depicted. The linear diagonal parts of each curve result from unloading and reloading of the sample. The Young's modulus is obtained as slope of these parts by average. The Young's modulus of samples E was measured to be 204 ± 4 GPa, and for sample F Young's modulus was found to be 171 ± 4 GPa (see Table 2).

Sample F had a yield strength ($\sigma_{0.2\%}$) of 450 MPa and an ultimate tensile strength (σ_{UTS}) of 670 MPa. By contrast,

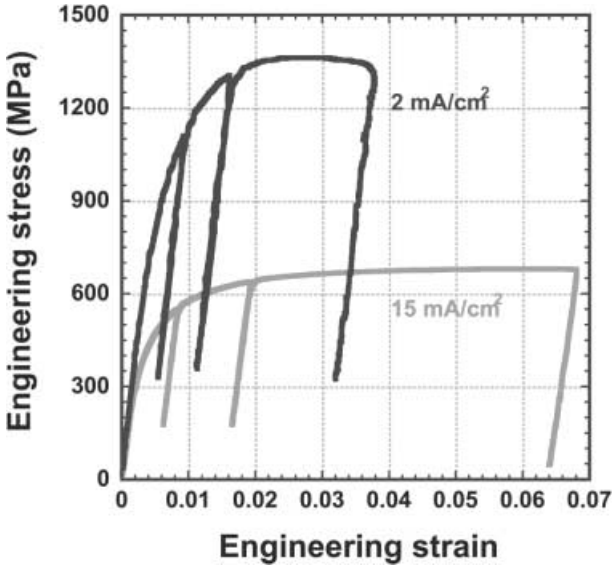

Fig. 5. Stress–strain diagrams of samples E and F. The linear diagonal curve parts are subject to unloading and reloading of the sample to determine Young's modulus

Table 2. Results of measurements of Vickers hardness and tensile testing of samples E and F

Sample	E 2.0 mA/cm^2	F 15.0 mA/cm^2
Indentation hardness (Vickers)	433 HV0.5	274 HV0.5
Yield strength (MPa)	995	450
Ultimate tensile strength (MPa)	1385	670
Young's modulus (GPa)	204 ± 4	171 ± 4

the yield strength of the sample E was measured to be 995 MPa and the ultimate tensile strength 1385 MPa (see Table 1).

4 Discussion

The $\theta/2\theta$-measurements of the four 15 μm thick nickel layers A to D (Fig. 1) show a dependency of their crystallographic properties with respect to the mean current density [3]. According to the relative peak intensities (see Table 1) the nickel (2 2 0) peak decreases, whereas the (2 0 0) peak increases with increasing mean current density. This indicates a change from a ⟨1 1 0⟩-texture to a ⟨1 0 0⟩-texture with increasing mean current density. For mean current densities of 10 mA/cm^2 and above the intensities of the nickel peaks show similar values. Sample F electrodeposited with a mean current density between sample C and D shows the relative peak intensities of the (1 1 1) and (2 0 0) peak which are comparable to those of sample C and D. In contrast, the (2 2 0) peak shows low intensity compared to C and D. Although samples E and A were deposited at similar mean current densities $\theta/2\theta$-XRD of sample E does not show a sharp texture compared to sample A. But a weak ⟨1 1 0⟩-texture can be determined in sample E using texture analysis (see Fig. 2).

The crystallographic properties of the four 15 μm thick samples A to D agree with the results of Amblard et al. [7]. They observed a relationship between the texture and current density as well as pH of electroplated nickel layers from a sulphate based electrolyte (Watts electrolyte). The texture shift from ⟨1 1 0⟩-orientation at low current densities to ⟨1 0 0⟩-orientation at high current densities was explained by a mechanism of specific inhibition. At low current densities the growth of nickel crystallites is inhibited by adsorbed hydrogen while the ⟨1 0 0⟩-texture at high current densities is the result of uninhibited growth. The samples E and F show a similar tendency but sample E does not show strong ⟨1 1 0⟩-texture compared to sample A.

As discussed by Amblard et al. [10] statistically oriented electroplated nickel was observed in cases were stronger inhibition processes like precipitation of nickel hydroxide overcome or disturb the mechanism of adsorbed hydrogen at low current densities. As texture seems to be strongly related to surface adsorption processes, bath temperature and electrolyte stirring have strong effect. Also organic compounds in traces are known to interact with adsorbed hydrogen as well as raising pH in the double layer. Compared to the experimental set-up of Amblard et al. [7] our electroplating process is different in some aspects. Wetting agents are necessary to ensure void free depositions and wetting even in deep high aspect ratio cavities. The hydrodynamic conditions using micro structured 4″-wafers are different to those of small polished rotating disk electrodes (RDE) as used in [7].

In case of sample E a lower mean current density than in sample A was used. With respect to the discussed aspects a competition between statistically and ⟨1 1 0⟩-textured growth may lead to the observed weak ⟨1 1 0⟩-texture of sample E.

The cross sectional views of sample E and F (Fig. 3) confirm the assumptions of the discussed inhibition-growth model as they show typical morphology relating to Fischer's classification [11]. According to Fischer sample E corresponds to a field-oriented texture type which is related to inhibited growth. Sample F corresponds to a base-oriented reproduction type related to less inhibited electrocrystallization. Diagonal etch lines can be related to {1 1 1}-planes 45° towards direction of growth.

Measurement of Vickers hardness (Fig. 4) gives information about the plastic flow behavior of the tested material. The samples show a relation between indentation hardness and mean current density. With increasing mean current density the indentation hardness decreases.

The values of indentation hardness are confirmed by the values from tensile testing of samples E and F. According to the high strength values of sample E and the low strength values of sample F, respectively sample E is found to behave brittle, whereas sample F shows ductile behavior. Dislocation theory [12] is usually used to explain plastic flow of metals exposed to shear or tensile stress. Following this argumentation the unhindered motion of dislocations is necessary for plastic deformation with minimum shear stress. The fine grained sample E possesses more grain boundaries compared to sample F (see Fig. 3). These obstacles for dislocation motion contribute to Hall–Petch strengthening. This finding is consistent

with the work of Cho et al. [13], who have shown that low current densities result in finer grain sizes and highly twinned grains.

An additional effect contributing to the easy plastic flow of sample F could result from its texture. Indentation hardness is measured by applying a force perpendicular to the sample surface. Direction of force and the ⟨1 0 0⟩-orientation are the same. According to [12] in cubic-face centered (fcc) metals like nickel {1 1 1} planes slip in ⟨1 1 0⟩-direction for plastic flow. In a strong ⟨1 0 0⟩-textured fcc metal this slip system has a tilt angle of 45° towards direction of force which is the ideal case for plastic flow, according to Schmidt's law. Because of the large crystallites grain boundaries have less effect compared to sample E. With respect to the cubic symmetry of the nickel crystallites also in tensile testing the slip system can be applied with minimal tensile stress in ⟨1 0 0⟩-textured nickel.

The Young's modulus of the micro tensile samples F can also be explained by considering the crystallographic texture of these specimens. The in-plane modulus for ⟨0 0 1⟩ out-of-plane textured nickel samples has been shown to vary between 171 and 177 GPa, see for example [13] and [14], and the values and texture measurements reported in this paper are in very good agreement with these previous studies. The modulus of the micro tensile samples E is consistent with literature values for the Young's modulus of random polycrystalline nickel (207 GPa), see for example [14].

Qualitatively, the presented results agree previously published in [4–6]. Young's modulus decreases with increasing mean current density. However, Young's modulus was determined by a factor approximately ten times lower compared to the values presented here and values known from literature. After redesign of tensile samples and evaluation of the used tensile testing equipment it was concluded that the testing equipment cannot be used for measuring metallic samples with sufficient accuracy.

5 Conclusion

The mechanical properties of electroplated nickel strongly depend on the parameter mean current density used for deposition. Grain size and crystallographic texture can be explained by inhibition mechanisms of the electrocrystallization of electroplated nickel. At low mean current densities brittle layers with high Young's modulus and indentation hardness are obtained whereas at high current densities ductile layers are electrodeposited. For the application of movable surface micro structures with elastic behavior the deposition with low current densities should be preferred.

References

1. **Ehrfeld W** (1990) The LIGA Process for microsystems. Proc Microsystem Technology, p. 521. Springer, Berlin, Heidelberg, New York
2. **Maciossek A; Löchel B; Quenzer HJ; Wagner B; Schulze S; Noetzel J** (1995) Galvanoplating and sacrifial layers for surface micromachining. Microelectronic Eng 27: 503–508
3. **Fritz T; Mokwa W; Schnakenberg U** (2001) Material characterization of electroplated nickel structures for microsystem technology. Electrochim Acta 47,1–2: 55–60
4. **Krüger C; Fritz T; Leuerer T; Mokwa W; Schnakenberg U** (2000) Micro-springs for temporary chip connections. Sensors and Actuators 85: 371–376
5. **Fritz T; Leuerer T; Krüger C; Mokwa W; Schnakenberg U** (2000) Mechanical properties of electroplated nickel. Dig Micro Materials Micro Mat 2000, 3rd International Conference and Exhibition, Berlin, Germany, pp. 752–755. Dresden: ddp goldenbogen
6. **Fritz T; Krüger C; Mokwa W; Schnakenberg U** (2000) Mechanische Charakterisierung galvanisch abgeschiedener Nickelstrukturen für die Mikrosystemtechnik. Galvanotechnik 91: 2894–2898
7. **Amblard J; Froment M; Spyrelis N** (1977) Origine de textures dans les depots electrolytiques de nickel. Surf Technol 5: 205–234
8. **Sharpe WN Jr** (1989) NASA Report No. 101638
9. **Zupan M; Hemker KJ** (2001) Application of Fourier analysis to the laser based interferometric strain/displacement gage. Experimental Mechanics (submitted)
10. **Amblard J; Epelboin I; Froment M; Maurin G** (1979) Inhibition and nickel electrocrystallization. J Appl Electrochem 9: 233–242
11. **Fischer H** (1954) Elektrolytische Abscheidung und Elektrokristalisation von Metallen. Springer, Berlin, Heidelberg, New York
12. **Kittel CH** (1983) Introduction to Solid State Physics. Wiley, New-York
13. **Cho HS; Dirras G; Babcock WG; Last H; Hemker KJ** (2001) Tensile properties of LIGA Ni structures for a safety and arming device. Microsystem Technologies, submitted. Springer, Berlin, Heidelberg, New York
14. **Hemker KJ; Last HR** (2001) Mater Sci Eng A (in press)
15. ASM International Handbook Committee (1990) Metal Handbook. 10th edn. vol. 2, p. 777. ASM International